Optics Communications 309 (2013) 212–220

Contents lists available at ScienceDirect

Optics Communications

journal homepage: www.elsevier.com/locate/optcom

Free space optical communication performance analysis with focal plane based wavefront measurement

Wei Liu [a], Wenxiao Shi [a,*], Bin Wang [b], Kainan Yao [b,c], Yaowen Lv [b,c], Jihong Wang [a]

[a] College of Communication Engineering, Jilin University, 5372 Nanhu Road, Changchun 130012, PR China
[b] Changchun Institute of Optics, Fine Mechanics and Physics, Chinese Academy of Sciences, 3888 Nanhu Road, Changchun 130033, PR China
[c] Graduate School of Chinese Academy of Sciences, Beijing 100039, PR China

ARTICLE INFO

Article history:
Received 5 December 2012
Received in revised form
4 July 2013
Accepted 4 July 2013
Available online 18 July 2013

Keywords:
FSO communication
Wavefront measurement
Aberrations compensation
Coupling efficiency
BER

ABSTRACT

In order to decrease the Bit Error Rate (BER) and increase coupling efficiency of free space optical (FSO) communication system, we compute and compensate the wavefront aberrations of the laser signal with the wavefront measurement method based on the focal plane proposed in this paper. The aberrations of laser signal are calculated based on the two images which are respectively generated from focal plane (PF) channel and the defocused plane (DF) channel. Assuming the On–Off Keying (OOK) modulation is used under the condition of weak turbulence, the fundamental of wavefront measurement method based on focal plane is introduced. By numerical simulation, we analyze the variation trend of coupling efficiency and BER, using the method we proposed to measure and compensate the wavefront aberrations for the FSO communication system. The experiment results show that the wavefront measurement error can reach nearly 0.004 wavelengths, the average coupling efficiency increases from 10.32% to 63.82%, and the average BER of FSO communication system decreases from 10^{-5} to 10^{-13}.

1. Introduction

Free space optical (FSO) communication system is an access technique with large capacity, wide bandwidth, high security and low cost [1–3]. It has been considered as an effective solution for the "last mile problem". In this system, the laser signal is transmitted through atmosphere, so the atmospheric turbulence is the major impairment which causes the atmosphere refractive index changed with time and space, and fluctuates both the amplitude and phase of the laser signal along the propagation path [4,5]. Therefore, the laser signal suffers from wavefront distortion, resulting in beam wander, beam scattering, scintillation and power fluctuations which seriously limits the coupling efficiency of the fiber-coupled FSO communication system [6,7], and severely reduces the Signal to Noise Ratio (SNR) [8–10], and thereby increase the BER. Adaptive optics (AO) system can effectively reduce the effects of atmospheric turbulence by correcting the wavefront aberrations and improve the FSO system performance [11,12]. There are three components in AO system: the wavefront sensor, wavefront controller and wavefront corrector. The wavefront sensor measures the wavefront distortion, and then feeds back the distortion to the wavefront controller. The wavefront controller controls the wavefront corrector to make real-time correction of wavefront distortion [13]. The way to measure the wavefront distortion is the key problem in the AO systems. The Shack–Hartmann wavefront sensor (SH–WFS) [14–16], which framework is shown in Fig. 1, is one type of sensors generally used in AO systems [17–19]. The framework of SH–WFS measures the wavefront by multiple spectroscopic with the microlens array, it cannot detect the laser intensity all the time, especially for near-ground remote transmission when the laser scintillation caused by atmospheric turbulence is strong.

Sensor-less wavefront measurement technology is developing rapidly, such as Stochastic Parallel Gradient Descent (SPGD) algorithm is proposed to control the wavefront correctors in AO systems. However, the control bandwidth is limited and control process is divergent in particular situation [20–24]. Other algorithm based on a transport of intensity equation-based numerical method is proposed [25], which is complicated due to reconstructing both the phase and intensity by numerical computation. Additionally, the surface plasmons are used to measure wavefront distortion in FSO communication system [26]. The method using on-shot and offline camera-based far-field measurements improve the wavefront measurements performance in high-energy laser systems, but its application is limited due to the complex structure [27].

In this paper, we propose a new measurement method based on focal plane which is different from the traditional wavefront

* Corresponding author. Tel.: +86 13504333501.
E-mail address: swx@jlu.edu.cn (W. Shi).

0030-4018/$ - see front matter © 2013 Elsevier B.V. All rights reserved.
http://dx.doi.org/10.1016/j.optcom.2013.07.022

measurement based on pupil plane. Compared with SH–WFS, it can avoid power loses by less spectroscopic. In order to prove the availability of our method, we measure the wavefront aberrations with the method and compare the results with the known aberrations which are randomly introduced by the numerical simulation and the measurement error can reach nearly 0.004 wavelengths. By numerical simulation, we deeply analyze the influence on the performance of FSO system caused by our method. The results show that average coupling efficiency increases from 10.32% to 63.82%, the average BER of FSO system decreases from 10^{-5} to 10^{-13}.

2. System model

The AO system is significant to improve the FSO communication system performance. It includes wavefront sensor, wavefront controller and wavefront corrector. Wavefront sensor measures wavefront aberrations which are the feedback signals for wavefront controller. Wavefront corrector real-time compensates the wavefront aberrations according to the control command from wavefront controller. So the measurement of wavefront aberrations is very important. In this paper we propose a new method based on focal plane to measure the wavefront aberrations. The functional block diagram of FSO system with our method to detect the wavefront aberrations is shown in Fig. 2. As the Fig. 2 shows, the laser signal through the atmospheric turbulence is divided into two beams, one is used for wavefront measurement and the other is coupled into a single mode fiber and received by the optical receiver.

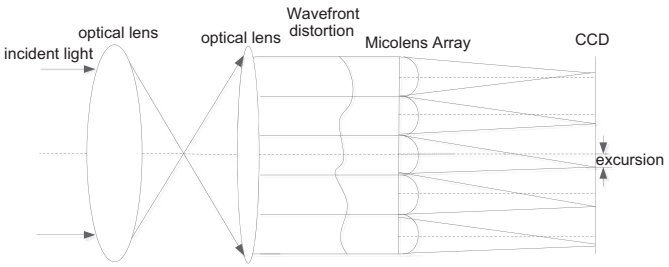

Fig. 1. Framework of SH-WFS.

The theory of the wavefront measurement method based on focal plane is shown in the dotted line of Fig. 2. The convergent laser signal is split by a spectroscope, one is received by the focal plane (FP) channel and the other is received by the defocus plane (DF) channel. The beams of laser signal are imaged respectively in the two channels with Charge Coupled Device (CCD) camera. Then we can calculate the wavefront aberrations of the laser signal according to the information of the two images. The wavefront aberrations we got are fed back to control the wavefront corrector for compensating aberrations and recovering wavefront phase.

3. The numeral model of focal plane based wavefront measurement method

At the transmitting terminal, the laser source can be approximated as a pointolite. We use OOK modulation method, making laser pulse in each information bit at “on” or “off” status. We use “1” to represent having laser pulse at “on” status and “0” represent none laser pulse at “off” status. The atmosphere and antenna of FSO system can approximate linear spatially invariant system [28]. The imaging formula of Gaussian Noise model is:

$$d(x) = f(x) * h(x) + n(x) \tag{1}$$

where $d(x)$ represents target laser signal image, $f(x)$ represents ideal image of the target, $h(x)$ represents the Point Spread Function (PSF), $n(x)$ represents the Gaussian noise. This system applies Additive White Gaussian Noise (AWGN) model. Apply Fourier Transform to both sides of Eq. (1):

$$D(u) = F(u)H(u) + N(u) \tag{2}$$

where $D(u)$, $F(u)$, $H(u)$ and $N(u)$ are the frequency domain of $d(x)$, $h(x)$, $f(x)$ and $n(x)$.

There are known phase differences between the two channels which are used in our method to image laser signal. In this paper we take the defocusing amount as known phase difference, and get the laser signal images by CCD. For convenience of illustration, the two channels are separately defined as FP channel and DP

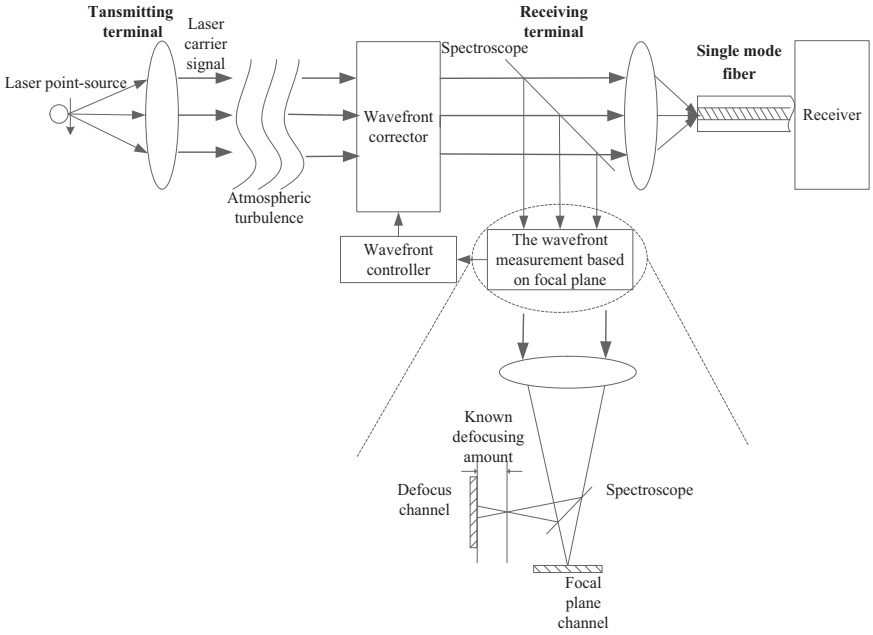

Fig. 2. Functional block diagram of the system.

channel. The FP channel means the imaging plane is at the focus plane; the DP channel means there is a known optical path difference between the imaging plane and the focus plane, which causes a known defocusing amount at phase plane. The FP channel can be represented as Eq. (3) and the DP channel is expressed as Eq. (4)

$$D_1(u) = F(u)H_1(u) + N_1(u) \tag{3}$$

$$D_2(u) = F(u)H_2(u) + N_2(u) \tag{4}$$

where, $D_1(u)$, $H_1(u)$ and $N_1(u)$ are the frequency domain of target laser signal image, the PSF and the noise in the FP channel. Additionally, $D_2(u)$, $H_2(u)$ and $N_2(u)$ separately express the frequency domain of target laser signal image, the PSF and the noise in the DP channel.

Based on Fourier Optical Theory, the relationship between the PSF and the pupil function of the pointolite is shown as:

$$h(x) = |\mathscr{F}^{-1}\{P(u)\}|^2 \tag{5}$$

where $P(u)$ represents pupil function as

$$P(u) = A(u)e^{i(\phi(u))} \tag{6}$$

where, $A(u)$ is the pupil amplitude function, and the unknown aberrations $\phi(u)$ is the pupil wave phase, which can be decomposed as the sum of Zernike polynomial [29]

$$\phi(u) = \theta(u) + \sum_{m}^{M} \alpha_m Z_m(u) \tag{7}$$

where $Z_m(u)$ is Zernike base of the m-th item, α_m is the Zernike factor of the m-th item, $\theta(u)$ is the known fixed defocused aberration. Therefore, the unknown phase difference can be got by calculating the coefficient of the Zernike polynomial, thus the PSF $h(x)$ can be got from the Eqs. (5) and (6).

In the condition of Gaussian noise model, the mean-square deviation between the target laser signal image and the images of the two channels can be represented by likelihood function:

$$L(u,\alpha) = \frac{\sum_{u}\left(\sum_{n=1}^{2}|D_n(u) - F(u)H_n(u)|^2 + \gamma|F(u)|^2\right)}{2N} \tag{8}$$

where $D_n(u)$ is $D(u)$ of the n-th channel, $H_n(u)$ is $H(u)$ of the n-th channel, N is the sum of image pixels, α is the Zernike factor, γ is the non-negative regularization coefficient. Based on the Maximum Likelihood Estimation (MLE), the target estimation as independent pilot process is separate with the phase estimation. The target function which has no relation with the real target can be expressed as:

$$L_M(u,\alpha) = \frac{\sum_{u}\left(\sum_{n=1}^{2}|D_n(u)|^2 - \left(|\sum_{i=1}^{2}D_n(u)H_n^*(u)|^2/\gamma + \sum_{n=1}^{2}|H_n(u)|^2\right)\right)}{2N} \tag{9}$$

where $L_M(u,\alpha)$ is the MLE for $L(u,\alpha)$. Hence, the ideal image of the target $f(x)$ can be represented as:

$$f(x) = \mathscr{F}^{-1}\left\{\frac{\sum_{n=1}^{2}D_n(u)H_n(u)^*}{\gamma + \sum_{n=1}^{2}|H_n(u)|^2}\right\} \tag{10}$$

The minimal Zernike coefficient of the target function can be got by using optimal estimation iteration. We can calculate the aberrations and get the point spread function.

In this paper, we use numerical simulation to get the images from the FP channel and the DP channel, and calculate the wavefront aberrations to recover the phase of the laser signal.

4. Analysis of the coupling efficiency and BER

Generally, the received laser signals are coupled into a single mode fiber, so the coupling efficiency has significant influence on the performance of FSO system. The coupling efficiency of the single mode fiber is defined as the ratio of the average power coupled into the fiber to the average power in the receiver aperture plane [30], it is given by:

$$J \propto \frac{|\iint A_f(r)M_0^*(r)d^2r|^2}{\iint A_f(r)A_f{}^*(r)d^2r \times \iint M_0(r)M_0^*(r)d^2r} \tag{11}$$

where, $A_f(r)$ is the Fourier transform of the single-mode fiber optical field, $M_0(r)$ is the incident optical field in the focal plane, $A_f(r)$ and $M_0(r)$ are complex quantities. However, the Eq. (11) is too complex to calculate, we can use the Strehl Ratio to approximate the average coupling efficiency [31], and the Strehl Ratio is given by:

$$ST \propto |A_f(r_0)|^2 \tag{12}$$

where, r_0 is the desired on-axis location of the center of the fiber. In this paper, we calculate the Strehl Ratio of the laser signal images in the focal plane to analyze the coupling efficiency.

Effect of atmospheric turbulence on FSO system is described based on the Theory of Kolmogorov and Rytov [32], according it, the wave equation of the laser beam in atmosphere turbulence is:

$$u(\bar{r}) = A(\bar{r})\exp[i\phi(\bar{r})] = u_0(\bar{r})\exp[\Phi_1] \tag{13}$$

where, $A(\bar{r})$ is the amplitude of the laser signal influenced by atmospheric turbulence; $u_0(\bar{r})$ is laser signal without the turbulence; Φ_1 is the perturbation factor, $u_0(\bar{r})$ can be shown as:

$$u_0(\bar{r}) = A_0(\bar{r})\exp[i\phi_0(\bar{r})] \tag{14}$$

where $A_0(\bar{r})$ is the amplitude of laser signal regardless of the atmospheric turbulence; the perturbation factor Φ_1 can be represented as:

$$\Phi_1 = \ln\left[\frac{A(\bar{r})}{A_0(\bar{r})}\right] + i[\phi(\bar{r}) - \phi_0(\bar{r})] = \chi + i\zeta \tag{15}$$

where χ and ζ are the logarithmic amplitude fluctuation and phase fluctuation of the laser signal caused by atmosphic turbulence. Both the amplitude fluctuation and phase fluctuation have a great impact on the SNR and BER of FSO system, we only consider the phase fluctuation in this paper.

Assuming the intensity of atmospheric turbulence is uniform, the logarithmic intensity fluctuation of laser signal can be represented as:

$$\sigma_{\ln R}^2 = 1.23C_n^2k^{7/6}L^{11/6} \tag{16}$$

where $k = 2\pi/\lambda$ is the wave number, L is the transmission distance, C_n^2 is the structure constant of refractive index. Under the condition of weak atmospheric turbulence, $C_n^2 \leq 10^{-14}m^{-2/3}$.

For BER of FSO system, the average received power, scintillation intensity and the receiver noise are the three most important factors. Here, we only consider the noise which caused by atmospheric turbulence. The logarithmic amplitude is given as:

$$\chi = \ln\left[\frac{A(\bar{r})}{A_0(\bar{r})}\right] = \ln\left[\frac{A_0(\bar{r}) + A_i(\bar{r})}{A_0(\bar{r})}\right] = \ln(1+\varepsilon) \tag{17}$$

In Eq. (17), $A_i(\bar{r})$ is the amplitude of noise, and $\varepsilon = A_i(\bar{r})/A_0(\bar{r})$ is the amplitude ratio between noise and signal.

Under the condition of weak atmospheric turbulence, ε can be considered as infinitesimal factor, so $\chi = \ln(1+\varepsilon) \approx \varepsilon$. Then, for the plane wave, the relation between χ and ε can be obtained as

$$<\varepsilon^2> = <\chi^2> = 0.31C_n^2k^{7/6}L^{11/6} \tag{18}$$

Therefore, the SNR of FSO system can be represented as

$$SNR = \frac{I_0}{< I_i >} = \frac{< A_0^2(\bar{r}) >}{< A_i^2(\bar{r}) >} = \frac{1}{< \varepsilon^2 >} = (0.31 C_n^2 k^{7/6} L^{11/6})^{-1} \quad (19)$$

where, I_0 is the intensity of laser signal, and $< I_i >$ is the average of noise intensity. Using OOK modulation method in the FSO system, the laser signal after collimation at transmitter can be regarded as plane wave [33]. The BER of the FSO system can be represented as:

$$BER = \frac{1}{2} erfc\left(\frac{Q}{\sqrt{2}}\right) \approx \frac{\exp(-Q^2/2)}{Q\sqrt{2\pi}} \quad (20)$$

where, $Q = (A_1 - A_0/\sigma_1 - \sigma_0)$, A_1 and σ_1 are the laser signal power and noise power when the received bit is "1"; A_0 and σ_0 are the laser signal power and noise power when the received bit is "0". In the FSO system, for the OOK modulation, $A_0 = 0$, $A_1 = < A_0(r) >$, $\sigma_1 + \sigma_0 = < A_i(r) >$. Hence, the SNR can be transformed as [34]:

$$SNR = \frac{< A_1^2 >}{< \sigma_1^2 + \sigma_0^2 >} = Q^2 \quad (21)$$

Therefore, under the condition of weak turbulence, the relationship between SNR and BER can be expressed as:

$$BER = \frac{\exp(-SNR/2)}{\sqrt{2\pi SNR}} \quad (22)$$

5. Numerical simulation

In the condition of weak atmospheric turbulence, we get laser signal images which are added known random aberrations by numerical simulation. Firstly, the known random aberrations are added to the laser signal, and then the laser signal images for both FP channel and DP channel are given respectively. Secondly, the wavefront aberrations according to the information of the two images are calculated. Thirdly, the wavefront measurement precision is analyzed by comparing the calculated wavefront aberrations and known random aberrations. Finally, we estimate the coupling efficiency and the BER of FSO system before and after aberrations correction respectively.

The numerical simulation uses laser with center wavelength $\lambda = 1060$ nm, receiving antenna focal length $f = 3.7$ m, aperture $d = 0.2$ m, the pixel size of CCD is 9.9 μm. We only consider the wavefront phase difference introduced by atmosphere turbulence. The integration time is 500 μs, we make ten simulation experiments, then take the first group as an instance to give a detailed analysis. From the 4th to the 18th Zernike aberrations are randomly introduced, they are shown in Table 1.

The distribution of wavefront after added random aberrations is shown in the Fig. 3.

The statistical property of wavefront phase after added random aberrations is described by Root-Mean-Square (RMS) value and Peak-to-Valley (PV) value:

RMS = 0.30360 wavelengths
PV = 1.72327 wavelengths

Assuming the defocusing amount between FP channel and the DP channel is 0.5 mm, we calculate the wavefront aberrations according to information of the two images from the FP channel and the DP channel. And we get the reconstructed image by compensating the wavefront phase, as shown in Fig. 4. Where Fig. 4(a) is the image of FP channel after introducing aberrations; Fig. 4(b) is the image of DP channel after introducing aberrations; Fig. 4(c) is the reconstructed image after aberrations compensation.

The wavefront aberrations can be caculated based on the laser signal images obtained from FP channel and DP channel in Fig. 4 by the wavefront measurement we proposed. The random introduced aberrations and residual errors $\varepsilon(i)$ are listed in Table 2. Where, the residual errors are the difference between introduced aberrations and calculated aberrations.

The measured wavefront distributions with our method are shown in Fig. 5. Compared with Fig. 3, the distributions of the calculated wavefront and the introduced random wavefront are nearly the same.

The statistical property of measured wavefront phase are listed below, including RMS value and PV value:

RMS = 0.30183 wavelengths
PV = 1.70519 wavelengths

Generally, The standard deviation of aberrations can be used as wavefront measurement errors [35], it can be represented as:

$$\sigma = \sqrt{\frac{\sum_{i=4}^{18} \{[\varepsilon(i)]^2\}}{N}} \quad (23)$$

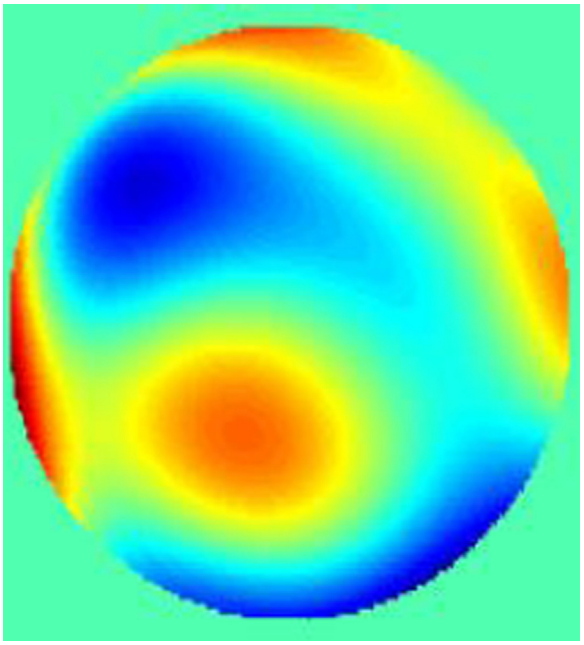

Fig. 3. Distribution of wavefront after added random aberrations.

Table 1
Fourteen items of random Zernike aberrations introduction.

Zernike item	4th item	5th item	6th item	7th item	8th item	9th item	10th item	11th item
Aberrations (Wavelengths)	0	−0.1561	0.0495026	−0.1989608	−0.0125863	0.0619762	−0.0111087	0.0394373
Zernike item	12th item	13th item	14th item	15th item	16th item	17th item	18th item	
Aberrations (Wavelengths)	0.066786	0.0597832	0.0738402	−0.0385882	0.0175494	0.0175494	0.0175494	

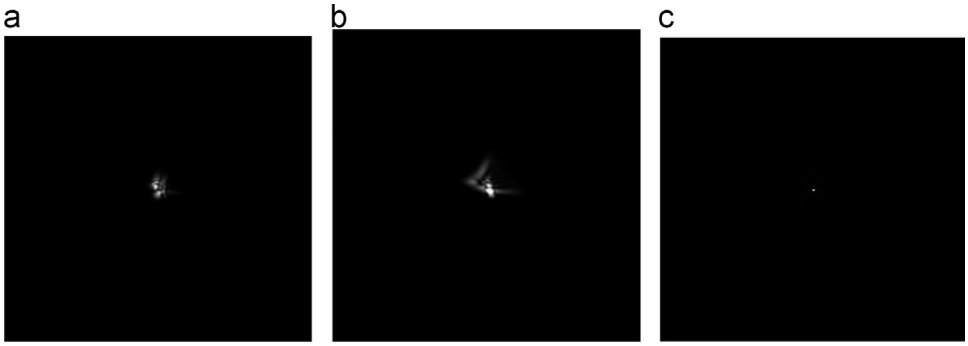

Fig. 4. Image in the focal plane channel, in the defocus channel and the reconstructed image. (a) Image in the focal plane channel (b) Image in the defocus channel (c) Reconstructed image.

Table 2
Comparative wavefront aberrations and residual errors.

Zernike item	Introduced Aberrations (Wavelengths)	Calculated Aberrations (Wavelengths)	Residual Errors (Wavelengths)
4th item	0	0.00313939	−0.0031399
5th item	−0.1561	−0.155396	−0.000704
6th item	0.04950264	0.0447157	0.0047864
7th item	−0.1989608	−0.19722	−0.0017408
8th item	−0.01258632	−0.0137221	0.00113578
9th item	0.06197616	0.0604521	0.00152406
10th item	−0.01110872	−0.00780411	−0.00330461
11th item	0.03943728	0.0359475	0.0034978
12th item	0.066786	0.0673635	−0.0005775
13th item	0.0597832	0.0627446	−0.0029614
14th item	0.07384024	0.0744827	−0.00064246
15th item	−0.03858824	−0.0394331	0.00084486
16th item	−0.06154288	−0.0627936	0.00125072
17th item	0.03910048	0.0391945	−0.00009402
18th item	0.01754944	0.0169168	0.00063264

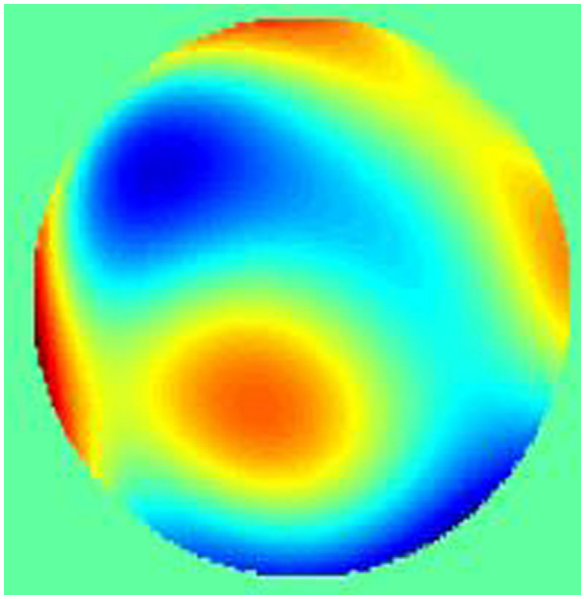

Fig. 5. Measured wavefront distributions with our method.

Table 3
Strehl Ratio.

	Without aberrations compensation system	After aberrations compensation
Strehl ratio	12.38%	63.84%

where, $\varepsilon(i)$ is residual error, N equals 15. According to Table 2, the standard deviation of aberrations is 0.00224 wavelengths. Therefore, the FSO wavefront measurement method based on focal plane can calculate wavefront aberrations accurately.

In order to estimate the coupling efficiency, we assume single-mode fiber coupling, and the fiber diameter is10 μm. Based on Eq. (12), for the pixel size of CCD approximately equal to the fiber diameter, the Strehl Ratio can be expressed as:

$$ST = \frac{|MAX[A(i)]|^2}{|\sum_{i=1}^{N}[A(i)^2]|} \tag{24}$$

where, $A(i)$ is the gray value of the i-th pixel, and N is the number of pixels. According to the Eq. (24),we can get the Strehl Ratio and they are shown in Table 3.

Under the condition of weak atmospheric turbulence, using OOK modulation condition, we can get the the SNR and BER of FSO system before and after wavefront aberrations compensation according to Eqs. (21) and (22).

The power distributions of the laser signal before and after wavefront aberrations compensation are shown in Fig. 6. Where, Fig. 6(a) is the power distributions of the laser signal without wavefront aberrations compensation; Fig. 6(b) is the power distributions of the laser signal after aberrations compensation; and Fig. 6(c) is the comparison of energy distributions before and after wavefront aberrations compensation.

As shown in Fig. 6(c), due to optical splitting, the received energy of FSO receiver without wavefront measurement is twice of that with wavefront measurement (assume the splitting rate is 50%). Therefore, in this paper, the comparison condition includes not only before and after wavefront aberrations compensation, but also without wavefront measurement.

We ignore the power loss generated by single mode fiber, and consider the receiver noise. The transmission speed is 10 Gbit; the

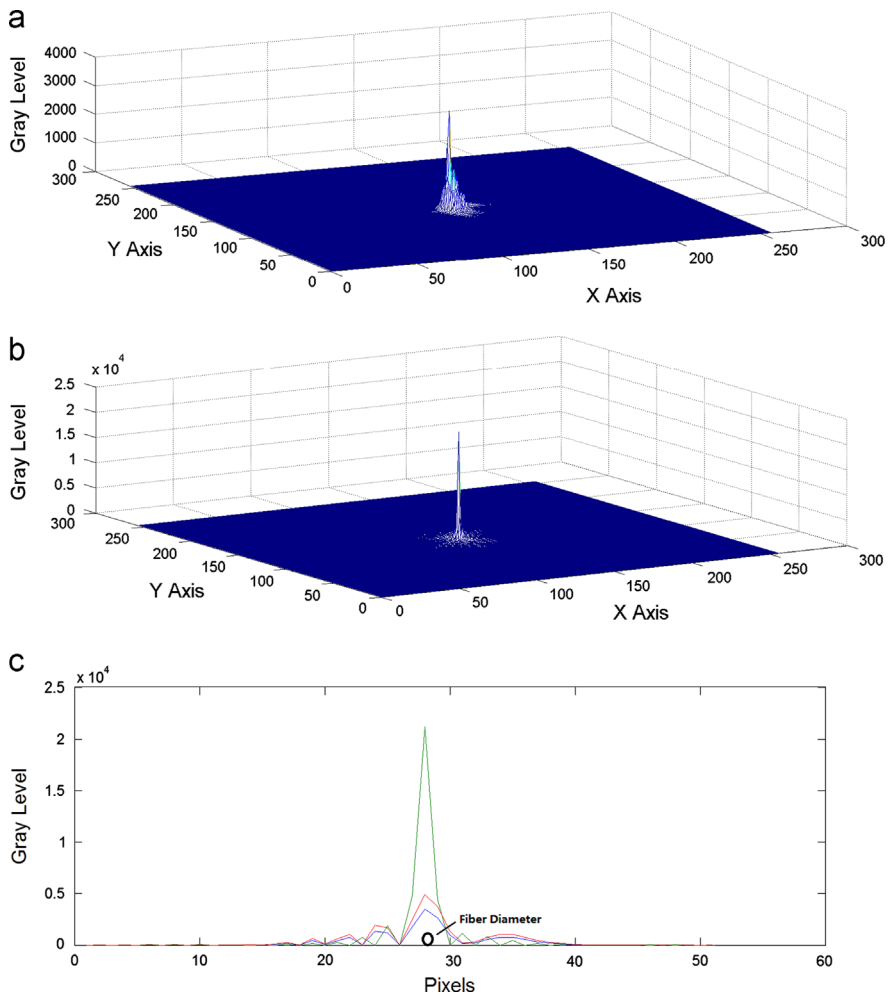

Fig. 6. Power distributions of laser carrier signal. (a) Power distributions of the laser carrier signal before compensating aberrations, (b) Power distributions of the laser carrier signal after compensating aberrations and (c) Results of comparing with the power distributions of the laser carrier signal before and after compensating wavefront aberrations. The green line denotes the power distributions of the laser carrier signal after compensating wavefront aberrations; the blue line shows the power distributions of the laser carrier signal before compensating wavefront aberrations; the red line shows the power distributions of the laser carrier signal without wavefront measurement system, the power is twice of that is before compensating aberrations. (For interpretation of the references to color in this figure legend, the reader is referred to the web version of this article.)

Table 4
Basic parameters of CCD.

Pixel size	9.9 μm × 9.9 μm
Resolution	256 × 256
Frame Rate	1076
Conversion Gain	34 μV/e$^-$
Saturation Charge	35000 e$^-$
QE	680 nm–100%, 1060 nm–6.25%
Sensitivity	3200 V m^2/W s
Optical Active Area	6.3 mm × 4.7 mm (1/2 inch)

Table 5
Power of laser carrier signal in the receiver.

	Before aberrations compensation	After aberrations compensation	Without wavefront measurement system
power of laser carrier signal	0.0104 mW	0.0634 mW	0.0208 mW

Table 6
SNR of the FSO system.

	Before aberrations compensation	After aberrations compensation	Without wavefront measurement system
SNR	10.3928	63.4047	20.7855

Table 7
BER of the FSO system.

Condition	BER
BER before Aberrations Compensation	6.8515×10^{-4}
BER without wavefront measurement system	8.5446×10^{-6}
BER after Aberrations Compensation	2.6823×10^{-16}

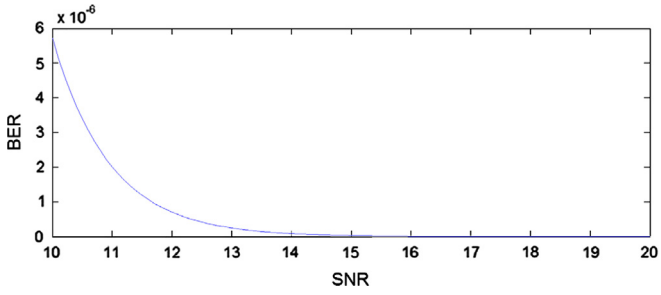

Fig. 7. Relationship between SNR and BER.

sensitivity is −30 dBm. Generally, the SNR can be shown as:

$$\mathrm{SNR} = \frac{E_b}{N_0} \tag{25}$$

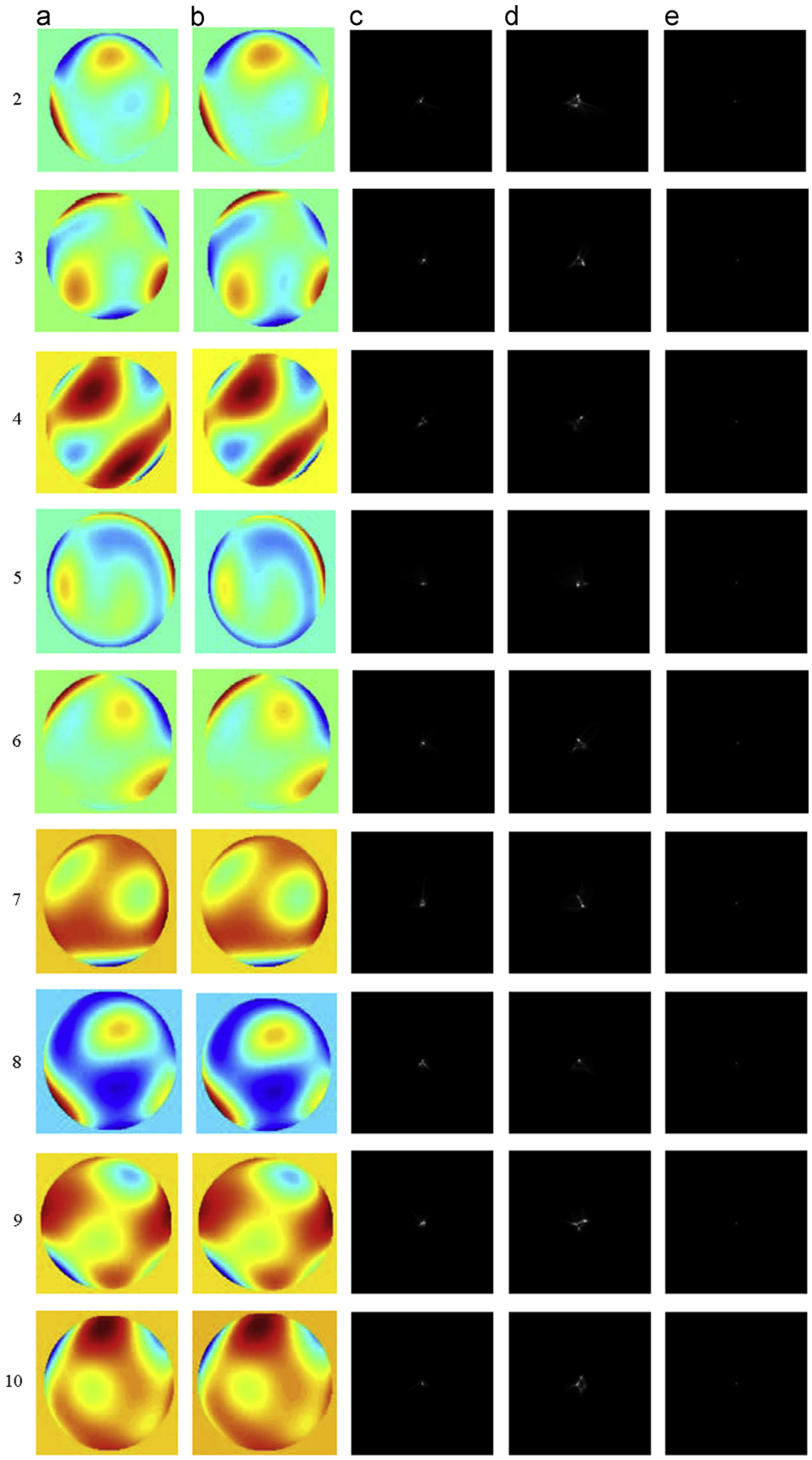

Fig. 8. Wavefront phase distributions and the laser carrier signal image.

where, E_b is laser signal power, and N_0 is noise power. The basic parameters of CCD used in this paper are shown in Table 4.

Since the pixel size of CCD approximately equal to the fiber diameter, the coupled power can be taken for the power of the images central point. Based on Table 4, the time of exposure is 500 μs, we can get the received power of laser signal. The results are shown in Table 5.

Then, the SNR can be calculated according to the Eq. (25), the results are shown as Table 6.

As Table 3 shows, the SNR of laser carrier before and after wavefront aberrations compensation is improved by 3.05 times. Then, the BER of the FSO system can be obtained based on the Eq. (20), the results are shown in Table 7. And the relationship between SNR and BER is shown in Fig. 7.

The BER of FSO system decreases from 10^{-6} to 10^{-16}, the proposed wavefront measurement method can measure the wavefront aberration accurately. It is significant to decrease the BER of the FSO system, thereby improve the FSO system performance.

Then, we analyze other 9 groups of simulation data in the same way, and the results are as shown in Table 8.

As shown in Table 6, the mean value of residual errors STD can represents the average error of the wavefront measurement. Therefore, the error of the wavefront measurement method based on focal plane is 0.004 wavelengths.

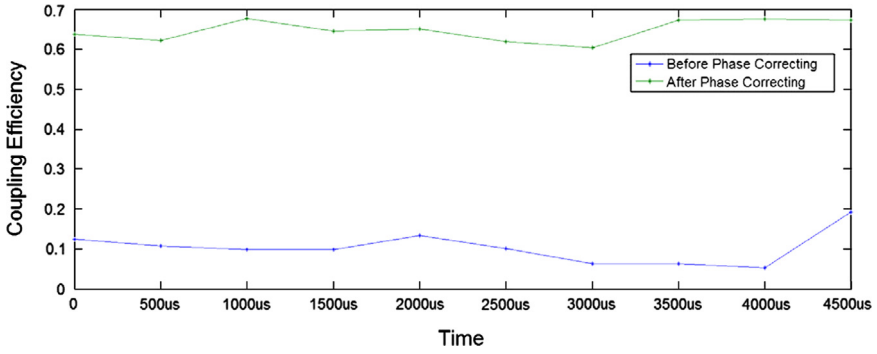

Fig. 9. Variation of coupling efficiency.

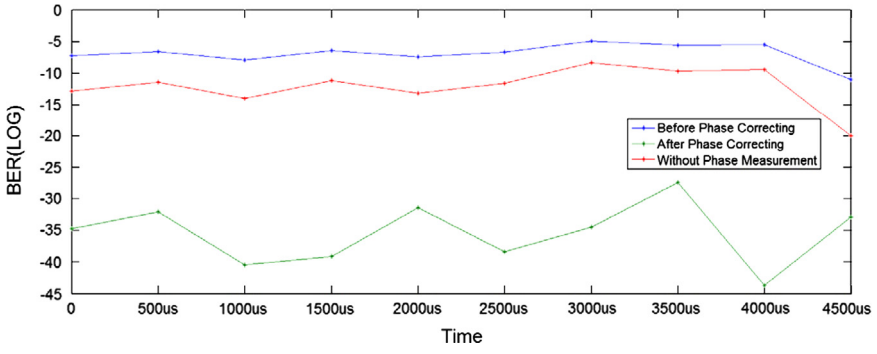

Fig. 10. Variation of BER.

Table 8
Simulation results.

Group	1	2	3	4	5	6	7	8	9	10	Mean
Introduced Wavefront RMS (wavelengths)	0.3036	0.4059	0.2403	0.362	0.3589	0.3829	0.3812	0.2867	0.311	0.3066	0.3339
Calculated Wavefront RMS (wavelengths)	0.3018	0.4084	0.2432	0.3636	0.3636	0.3829	0.3639	0.2837	0.3109	0.3118	0.3332
Aberrations STD errors (wavelengths)	0.0022	0.0043	0.0041	0.0046	0.0059	0.0034	0.008	0.0028	0.0024	0.0023	0.004
Introduced Wavefront PV (wavelenghs)	1.7233	3.4644	1.8186	1.853	3.1094	3.5504	3.3504	1.7167	2.1858	2.364	2.5136
Calculated Wavefront PV (wavelengths)	1.7052	3.5209	1.851	1.9306	3.2519	3.5559	3.1422	1.6705	2.1875	2.4196	2.5235
BER Before Aberrations Compensation	6.9×10^{-4}	1.4×10^{-3}	3.7×10^{-4}	1.6×10^{-3}	5.7×10^{-4}	1.3×10^{-3}	7.2×10^{-3}	3.5×10^{-3}	4.1×10^{-3}	1.6×10^{-5}	2.1×10^{-3}
BER Without Wavefront Measurement	2.9×10^{-6}	1.1×10^{-5}	8.1×10^{-7}	1.3×10^{-5}	1.9×10^{-6}	8.9×10^{-6}	2.3×10^{-4}	6.1×10^{-5}	7.9×10^{-5}	2.0×10^{-9}	4.1×10^{-5}
BER After Aberrations compensation	8.6×10^{-16}	1.2×10^{-14}	2.6×10^{-18}	9.9×10^{-18}	2.4×10^{-14}	2.1×10^{-17}	1.1×10^{-15}	1.2×10^{-12}	1.1×10^{-19}	5.1×10^{-15}	1.3×10^{-13}
Coupling Efficiency Before Aberrations Compensation	12.38%	10.67%	9.77%	9.87%	13.33%	10.13%	6.37%	6.28%	5.23%	19.21%	10.32%
Coupling Efficiency After Aberrations Compensation	63.84%	6.22%	67.78%	64.57%	65.09%	61.99%	60.38%	67.36%	67.64%	67.31%	64.82%

The wavefront phase distributions and the laser signal images of the other nine times experiments are shown in Fig. 8. Where, Fig. 8(a) expresses the wavefront phase distributions with introduced random wavefront aberrations. And Fig. 8(b) expresses the wavefront phase distributions with calculated wavefront aberrations. Fig. 8(c) shows the laser signal image in the FP channel, Fig. 8(d) indicates the laser signal images in the DP channel. Fig. 8(e) shows the reconstructed laser signal images after compensating aberrations.

The curve is drawn to describe the variation of the coupling efficiency and BER with time; the results are shown in the Figs. 9 and 10 and . Where, BER is plotted on the logarithmic scale.

According to the results of the ten simulation experiments, the focal plane based wavefront measurement method can measure the wavefront aberrations precisely. The average measurement error is 0.004 wavelengths. And after compensating the wavefront aberrations, the average BER of FSO system can descend from 4.09×10^{-5} to 1.26×10^{-13}, and the average coupling efficiency increase from 10.32% to 63.82%, thereby the FSO system performance is improved obviously.

6. Conclusions

A new wavefront measurement method based on focal plane is proposed in this paper which can effectively measure the wavefront aberrations in FSO systems. We use two laser images separately from FP channel and DP channel to calculate wavefront aberrations. Our method can measure the wavefront aberrations accurately by numerical simulation. The results indicate that wavefront measurement error is nearly 0.004 wavelengths. We also analyze the performance of FSO system, the results show that the average coupling efficiency increase from 10.32% to 63.82% and the BER of FSO system descends from 10^{-5} to 10^{-13}. Therefore, the FSO system performance is improved significantly.

The future research mainly focuses on the following two aspects: theory and experiment. The former is to improve the applicability of the algorithm by considering the model of extended light source. The latter is to optimize the algorithm using parallel processing technology, and then build experiment system to validate the algorithm proposed in this paper.

Acknowledgment

This work was supported by the National Natural Science Foundation of China (No.60972028).

References

[1] Fuxing Fu, Bin Zhang, Optics Communications 284 (2011) 4563.
[2] W.M. van Eekeren Adam, Klamer Schutte, Dijk Judith, Proceedings of SPIE 8355 (2012). (83550Q-1-83550Q-10).
[3] Sunil Vyas, P. Senthilkumaran, Optics Communications 283 (2010) 2767.
[4] Nadine Werth, Mathias S. Müller, Johann Meier, W.Koch. Alexander, Optics Communications 284 (2011) 2317.
[5] Kevin Murphy, Daniel Burke, Nicholas Devaney, Chris Dainty, Optics Express 18 (15) (2010) 15448.
[6] Niru K. Nahar, G. Rojas Roberto, IEEE Transaction 1 (10) (2011) 1553.
[7] Tao Wang, Ziyang Zhang, Fangfei Liu, Ye Tong, Jing Wang, Yue Tian, Min Qiu, Yikai Su, Optics Communications 282 (2009) 3464.
[8] Jaime A. Anguita, Jaime A. Anguita, Björn Hildner, Bane Vasic, Journal of Lightwave Technology 28 (7) (2010) 990.
[9] J.I. Davis, Applied Optics 5 (1) (1966) 139.
[10] Yuqiang Yang, Qiqi Han, Liying Tan, Guangyu Zhang, Journal of Lightwave Technology 29 (19) (2011) 2893.
[11] H. Song, R. Fraanje, G. Schitter, H. Kroese, G. Vdovin, M. Verhaegen, Optics Express 18 (23) (2010) 24070.
[12] R.K. Tyson, Principles of Adaptive Optics[M], 2nd ed., Academic, Boston, Mass, USA, 1998.
[13] Hongxin Huang, Takashi Inoue, Hiroshi Tanaka, Optics Express 19 (16) (2011) 15026.
[14] H. Richter, M. Greiner-Bär, N. Deßmann, J. Pfund, M. Wienold, Applied Physics Letters 031103 (101) (2012) 1. (2012).
[15] L. Seifert, H.J. Tiziani, W. Osten, Optics Communications 245 (2005) 255.
[16] Christian Schulze, Darryl Naidoo, Daniel Flamm, et al., Optics Express 20 (18) (2012) 19714.
[17] Tenghao Li, Mali Gong, Lei Huang, Yuntao Qiu, Qiao Xue, Applied Optics 5 (29) (2012) 7115.
[18] V. Lin, H.-C. Wei, H.-T. Hsieh, J.-L. Hsieh, G.-D.J. Su, Micro and Nano Letters 6 (7) (2011) 523.
[19] Minshan Jiang, Xiangyang Zhang, Carmen A. Puliafito, Hao F. Zhang, Shuliang Jiao, Optics Express 18 (21) (2010) 21770.
[20] Weyrauch Thomas, Vorontsov, A. Mikhail, Applied Optics 44 (30) (2005) 6388–6401.
[21] Han Liqiang, Shida Katsunori, Wang Qi, Li Zhiquan, Proceedings of SPIE 7513 (75130X) (2009) 1.
[22] Yi Zheng, Xiaohua Wang, Li Deng, Feng Shen, Xinyang Li, Optics Communications 284 (2011) 4975.
[23] H. Song, R. Fraanje, G. Schitter, H. Kroese, G. Vdovin, M. Verhaegen, Optics Express 18 (23) (2010) 24070.
[24] B.E. Kruschwitz, S.-W. Bahk, J. bromage, M.D. Moore, D. Irwin, Optics Express 20 (19) (2012) 20874.
[25] Bindang Xue, Shiling Zheng, Optik 122 (2011) 2101.
[26] Xiangmei Dong, Qiufang Zhan, Xiumin Gao, Tao Geng, Hanming Guo, Songlin Zhuang, Optik 123 (2012) 1901.
[27] B.E. Kruschwitz, S.–W. Bahk, J. Bromage, M.D. Moore, D. Irwin, Optics Express 20 (19) (2012) 20874.
[28] Wu Yuanhao, Wang Bin, Zha O Jinyu, Ming Ming, Lei Dong, Yang Qing-yun, Wang Ming-hao, Guo-qiang Wang, Optics and Precision Engineering 18 (8) (2010) 1849.
[29] Fengzhao Dai, Feng Tang, Xiangzhao Wang, Osami Sasaki, Peng Feng, Applied Optics 51 (2012) 20.
[30] Sumanta Mukhopadhyay, S. Gangopadhyay, S.N. Sarkar, Optik 2010 (121) (2010) 142.
[31] Thomas Weyrauch, Mikhail A. Vorontsov, John W. Gowens II, Thomas G. Bifano, SPIE 4489 (2002) 177.
[32] Arkadi Zilberman, Ephim Golbraikh, Norman S. Kopeika, Optics Communications 2010 (283) (2010) 1229.
[33] Stamatios V. Kartalopoulos, Proceedings of SPIE 6012 (2005) 1.
[34] Josue A. Lopez Leyva, Arturo Arvizu Mondragón, Edith García, Francisco J. Mendieta, Eduardo Alvarez Guzman, Philippe Gallion, Optical Engineering 51 (10) (2012) 1. (105002).
[35] Laurent M. Mugniera, Amandine Blanca, Jérôme Idierb. Phase, Advances in Imaging and Electron Physics 141 (2006) 1.